

FINITE ELEMENT ANALYSIS OF POST-TENSIONED CONCRETE BOX GIRDERS

Dr. Husain M. Husain
Professor / University of Tikrit

Mohanned I. Mohammed Hussein
M.Sc. / University of Baghdad

الخلاصة

تمت دراسة سلوك روافد الجسور الكونكريتية ذات المقاطع الصندوقية المسبقة الجهد تحت تأثير الأحمال قصيرة الأمد. تم استعمال العناصر الطابوقية ثلاثية الأبعاد ذات عشرين عقدة لتمثيل الكونكريت المكون لأعضاء الجسر الصندوقي. أما حديد التسليح فقد تم تمثيله باستخدام عنصر أحادي البعد مطمور في العنصر الكونكريتي الطابوقي. سلوك الكونكريت تحت الانضغاط مُثَّل بنموذج مرن-لدن مع تصعيد انفعالي يتبعه جزء لدن تام الذي ينتهي عند بداية تهشم الكونكريت. أما تحت الشد فقد استخدم نموذج توزيع الشقوق العمودية على محاور الإجهادات الرئيسية مع الأخذ بنظر الاعتبار مساهمة الكونكريت بين الشقوق والتغير في معامل القص في منطقة التشقق. تم تمثيل قوى الإجهاد في حبل الشد بتحويله إلى قوى مكافئة في العقد كما استخدمت طريقة لن (Lin). تم إدخال مصفوفة حبل الشد إلى المصفوفة الكلية باعتباره عنصر أحادي البعد مطمور في عنصر الكونكريت. كما دُرست حالة الخسائر القصيرة المدى في الجهد المسبق. وقد اخذ في التحليل ظاهرة الانزلاق-الربط عند سطح التلامس بين الكونكريت وحبل الشد. تمت دراسة وتحليل أنواع مختلفة من الجسور الصندوقية المسبقة الإجهاد وتم الحصول على توافق جيد بين النتائج المستحصلة من طريقة العناصر المحددة والنتائج العملية المتوفرة والنظرية من طرق أخرى.

ABSTRACT

The behavior of prestressed concrete box-girder bridges has been studied under short term loading. The 20-noded isoparametric three-dimensional brick elements have been used to model the concrete in the box-girder with its two cantilever flanges. The reinforcing bars are idealized as axial members embedded within the brick elements. The behavior of concrete in compression was simulated by an elastic-plastic work hardening model followed by a perfectly plastic response, which is terminated at the onset of crushing. In tension, a smeared crack model with fixed orthogonal cracks is used with the inclusion of models for the retained post-cracking stress and reduced shear modulus. The prestressing forces in the tendons are transformed into equivalent nodal forces and by Lin's method. The contribution of the prestressing tendon stiffness to the global stiffness matrix is considered by treating the tendon as axial member embedded within the brick element. Two types of short-term prestress losses are considered in this study. The bond-slip phenomenon at concrete-tendon is considered by reducing the tendon axial stiffness. Several examples of prestressed concrete box girders are analyzed and compared with available experimental and theoretical studies in order to demonstrate the validity and efficiency of the proposed method. Good agreements between the results are obtained.

INTRODUCTION

The relative economy of the box-girder bridges contributed greatly to its popularity, as it has relatively slender and unencumbered appearance. The structural simplicity of the box-girder bridges, particularly in continuous structures of medium to long spans, has been well demonstrated. The efficiency of the cross-section for positive and negative longitudinal bending moments, as well as torsional moments is apparent even to casual observer.

A box-girder bridge is a particular case of a folded plate structure where the plate elements are arranged to form a closed section. One of the main differences between the general shell and the box-girder (folded plate) is that in the general shell only two elements can meet at the same edge and the change of slope is smooth, while in the box-girder more than two elements can meet at the same edge at different inclinations. This causes a problem of slope discontinuity at corners^[4].

Problem of the slope discontinuity at corners by the use of brick elements does not exist due to existing of three translation degrees of freedom at each node.

The finite element method is the most versatile and appropriate numerical method that can cater for most of the following requirements: detailing, geometric and material behavior, loading characteristics, and the boundary conditions of the structure and any significant interaction among them. The finite element method employs an assemblage of discrete one, two and three-dimensional members to represent the structure. The structure is divided into elements that are only connected at their nodes which possess an appropriate number of degrees of freedom^[20].

This work is devoted to study the overall prestressed concrete box-girder bridges subjected to monotonically increasing load. In order to achieve this main objective, a computer program is used, which was originally developed by Al-Shaarbaf^[3], but modified to be capable of analyzing prestressed concrete box-girders, by developing a system to include the effect of prestressing in the element formulation.

FORMULATION OF FINITE ELEMENT

Concrete Idealization

The 20-noded hexahedral brick element is used in the current study to model the concrete^{[3][5]}. Each node of this element has three translation degrees of freedom u , v and w in the x , y and z directions respectively as shown in Fig. 1^[3]. The element employs the standard shape functions to define the displacement field^[68]. The displacements of the brick element are given by:

$$\begin{aligned} u(\xi, \eta, \zeta) &= \sum_{i=1}^{20} N_i(\xi, \eta, \zeta) \cdot u_i \\ v(\xi, \eta, \zeta) &= \sum_{i=1}^{20} N_i(\xi, \eta, \zeta) \cdot v_i \\ w(\xi, \eta, \zeta) &= \sum_{i=1}^{20} N_i(\xi, \eta, \zeta) \cdot w_i \end{aligned} \quad (1)$$

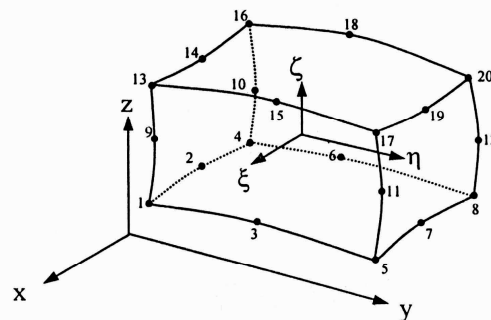


Fig. 1 20-Noded isoparametric brick element^[3].

Reinforcing Bar Idealization

The reinforcing bars are idealized as axial members embedded within the brick elements^[21]. Reinforcing bars are assumed to be capable of transmitting axial force only. The stiffness matrix of steel bars is added to that of the concrete to obtain the global stiffness matrix of the brick element. The shape functions of the brick element can be used to represent the displacements of the bar^[3]. For example,

$$u = \sum_{i=1}^{20} N_i(\xi) \cdot u_i$$

$$v = \sum_{i=1}^{20} N_i(\xi) \cdot v_i$$

where $N_i(\xi)$ is considered lying parallel to the local coordinate axis ξ with $\eta = \eta_c$ and $\zeta = \zeta_c$ (constant), Fig. 2.

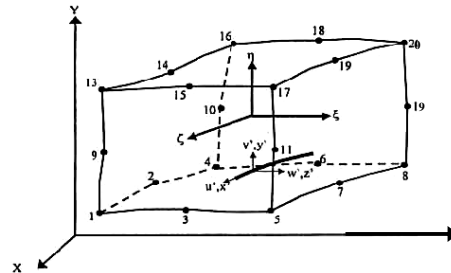


Fig. 2 Representation of reinforcement.

Bond and Bond-Slip Representation

For the embedded bar, either perfect a bond or a specified bond-slip relation is assumed. The present bond-slip formulation is based on the experimental results of Nilson^[48]. The bond-slip curve with $C=152$ mm (6 in.) is used (C , is distance from loaded face or face of crack), Fig. 3. Two polynomials are used to describe this curve, one for ascending portion, and the other for the descending part^[2]:

$$\frac{u}{\sqrt{f'_c}} = 0.083(7.5\alpha^3 - 25\alpha^2 + 27.5\alpha) \text{ for } 0 \leq \alpha < 1 \tag{3}$$

$$\frac{u}{\sqrt{f'_c}} = 0.083(2.5\alpha^3 - 15\alpha^2 + 22.5\alpha) \text{ for } \alpha \geq 1 \tag{4}$$

where u is the bond stress, MPa, f'_c , the cylinder compressive strength of concrete, $\alpha = \frac{\Delta}{\Delta_p}$, normalized slip, $\Delta =$ slip, mm, and $\Delta_p =$ slip at peak bond stress, mm.

To obtain the bond stiffness K_b , Eq. (3) and Eq. (4) are differentiated with respect to the slip Δ :

$$K_b = \frac{\partial u}{\partial \Delta} = 0.083 \frac{\sqrt{f'_c}}{\Delta_p} (22.5\alpha^2 - 50\alpha + 27.5) \text{ for } 0 \leq \alpha < 1 \tag{5}$$

$$K_b = \frac{\partial u}{\partial \Delta} = 0.083 \frac{\sqrt{f'_c}}{\Delta_p} (7.5\alpha^2 - 30\alpha + 22.5) \text{ for } \alpha \geq 1 \tag{6}$$

To account for bond slip, the steel axial stiffness is reduced by the bond slip stiffness^[12].

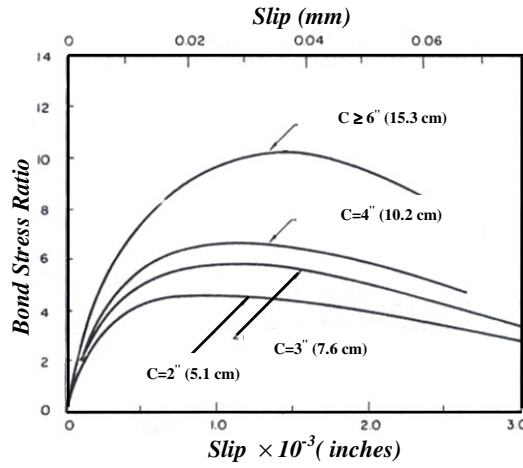


Fig.3 Representative bond stress-slip curves. [16].

General Nonlinear Solution Procedure

The **incremental-iterative** method is the most common technique used for solving nonlinear structural equations, due to their precise result^[8]. The **modified Newton-Raphson** method in which the stiffness matrix is updated at specified iterations of each increment of loading has been adopted. The convergence of the solution is controlled by a **force convergence criterion**. The numerical integration has been conducted by using $3 \times 3 \times 3 = 27$ -point Gaussian rule.

MODELING OF MATERIAL PROPERTIES

Modeling of Concrete

Behavior of Concrete in Compression

The behavior of concrete in compression is simulated by an elastic-plastic work hardening model followed by a perfect plastic response, which is terminated at the onset of crushing, Fig. 4. The plasticity model is illustrated in terms of the following constructions: the yield criterion, the hardening rule, the flow rule and the crushing condition.

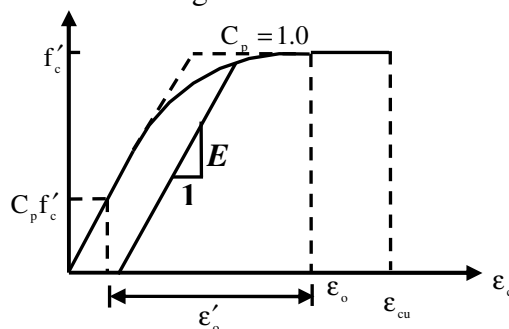


Fig. 4 Uniaxial stress-strain curve for concrete [3].

The state of stress must be scaled by an appropriate **yield criterion** to convert it to an equivalent stress that could be obtained from a simple experimental test. The yield criterion adopted in this work has been extensively used by many researchers^[3] and can be expressed as:

$$F(\{\sigma\}) = f(I_1, J_2) = \sqrt{\alpha I_1 + 3\beta J_2} = \sigma_o \tag{7}$$

where α , and β are material parameters to be determined by fitting biaxial test results, using the uniaxial compression test and the biaxial test under equal compressive stresses. I_1 , and J_2 are the first stress and second deviatoric stress invariants, and σ_o is the equivalent effective stress taken from uniaxial tests. The **hardening rule** defines the motion of the subsequent loading surface during plastic deformation. In the current study an isotropic hardening rule is adopted. The rule assumes that the yield surface expands uniformly without distortion as plastic flow occurs^{[6][7]}. Therefore, the subsequent loading functions may be expressed as:

$$F(\{\sigma\}) = C.I_1 + \sqrt{(C.I_1)^2 + 3\beta J_2} = \bar{\sigma} \tag{8}$$

where $c = \alpha/2\sigma_o$ and $\bar{\sigma}$ represents the stress level at which further plastic deformation will occur and it is termed as the effective stress or the equivalent uniaxial stress at that level.

The equivalent stress-strain relationships at various stages are:

1- Elastic stage:

$$\bar{\sigma} = E.\epsilon_c \quad \text{for} \quad \bar{\sigma} \leq C_p.f'_c \quad (C_p \text{ is the initial plasticity coefficient}) \tag{9}$$

2- Work-hardening stage:

$$\bar{\sigma} = C_p.f'_c + E \left[\epsilon_c - \frac{C_p.f'_c}{E} \right] - \frac{E}{2\epsilon'_0} \left[\epsilon_c - \frac{C_p.f'_c}{E} \right]^2 \quad \text{for} \quad C_p.f'_c \leq \bar{\sigma} \leq f'_c \tag{10}$$

3- Perfect plastic stage:

$$\bar{\sigma} = f'_c \quad \text{for} \quad \epsilon_c > \epsilon_0 \quad \text{or} \quad \epsilon_c > (2 - C_p) \frac{f'_c}{E} \tag{11}$$

where, ϵ_c is the effective total strain and ϵ'_0 is the total strain corresponding to the parabolic part of the curve given by:

$$\epsilon'_0 = \epsilon_0 - C_p \frac{f'_c}{E} \quad \text{or} \quad \epsilon'_0 = 2(1 - C_p) \frac{f'_c}{E} \tag{12}$$

To construct the stress-strain relationship in the plastic range, an associated **flow rule** is considered. This means that the plastic strain increment rate vector will be assumed to be normal to the yield surface, the plastic strain increment can be determined as^{[7][17]}:

$$d\{\epsilon_p\} = d\lambda \frac{\partial f(\sigma)}{\partial \sigma} \tag{13}$$

where $d\lambda$ is a parameter which determines the size of the plastic strain increment, and $\partial f(\{\sigma\})/\partial \{\sigma\}$ defines the direction of the plastic strain increment vector ($d\{\epsilon_p\}$) as normal to the current loading surface. The plastic multiplier, $d\lambda$ can be found as:

$$d\lambda = \left[\frac{\{a\}^T \cdot [D]}{H' + \{a\}^T \cdot [D] \cdot \{a\}} \right] \cdot d\{\epsilon\} \tag{14}$$

where $\{a\}$, the flow vector, is the yield function derivatives with respect to the stress components and $[D]$ is the elastic constitutive matrix. The elasto-plastic increment of total strain can be calculated as:

$$d\{\varepsilon\} = d\{\varepsilon_e\} + d\{\varepsilon_p\} \quad (15)$$

where $d\{\varepsilon_e\}$, and $d\{\varepsilon_p\}$ are the elastic and plastic strain components. The elastic strain increment is related to the stress increment by the elastic constitutive relationship, which is given by:

$$d\{\sigma\} = [D] d\{\varepsilon_e\} \quad (16)$$

Substitution of Eqs. (13), and (16) into Eq. (15) yields:

$$d\{\varepsilon\} = [D]^{-1} d\sigma + d\lambda \{a\} \quad (17)$$

$$d\{\varepsilon\} = [D]^{-1} d\{\sigma\} + \frac{\{a\}\{a\}^T [D]}{H' + \{a\}^T [D] \{a\}} \quad (18)$$

The crushing failure is a strain-controlled phenomenon. A failure surface in the strain space must be defined in order to take this type of failure into account. The **crushing criterion** can be obtained by simply converting the yield criterion, which is defined in Eq. (7) directly into strains instead of stress components^[7]:

$$\sqrt{\alpha I_1' + 3\beta J_2'} = \varepsilon_{cu} \quad (19)$$

where, I_1', J_2' , are the first strain and second deviatoric strain invariants, and ε_{cu} is the ultimate total strain extrapolated from the uniaxial compressive test results.

Behavior of Concrete in Tension

The behavior of concrete in tension is modeled as a linear elastic brittle material and the maximum tensile stress criterion is employed. A smeared crack model with fixed orthogonal cracks is adopted to represent the tensile fracture of concrete. The model is described in terms of a cracking criterion, post-cracking formulation and shear retention model. In order to describe this model, the following constituents must be defined. For a **cracking criterion**, cracking occurs if the principal tensile stress exceeds the limiting tensile strength of concrete^[3]. After cracking, the normal and shear stresses across the plane of failure and the corresponding normal and shear stiffnesses are reduced. However, the behavior of concrete between two adjacent failure planes remains linearly elastic, i.e., concrete is assumed to be transversely isotropic with planes of isotropy being perpendicular to the major principal stress direction which violates the cracking criterion. Thus, the elastic modulus in the direction of maximum tensile stress, σ_1 , is reduced. Because of the lack of interaction between the orthogonal planes caused by cracking, Poisson's ratio, ν , is set to zero and a reduced shear modulus $\beta_1 G$ is employed to model the shear strength deterioration. Therefore, the incremental stress-strain relationship in the local material axes may be expressed as:

$$\Delta\{\sigma\} = [D_{cr}] \Delta\{\varepsilon\} \quad (20)$$

where $[D_{cr}]$ is the material stiffness in local material axes.

In the present work, a **tension-stiffening model** is adopted, since the cracked concrete can still initially carry some tensile stresses in the direction normal to the crack. The gradual release of tensile stresses normal to the cracked plane is represented by an average stress-strain curve, Fig. 5, and expressed as^[3]:

$$1) \sigma_n = \alpha_2 \sigma_{cr} \left[\alpha_1 - \varepsilon_n / \varepsilon_{cr} \right] / \left[\alpha_1 - 1.0 \right] \text{ for } \varepsilon_{cr} \leq \varepsilon_n \leq \alpha_1 \varepsilon_{cr} \quad \dots(15)$$

$$2) \sigma_n = 0.0 \text{ for } \epsilon_n > \alpha_1 \epsilon_{cr} \quad \dots(16)$$

where σ_n and ϵ_n are the stress and strain normal to the crack plane, ϵ_{cr} is the cracking strain associated with the cracking stress σ_{cr} , α_1 and α_2 are the tension-stiffening parameters, (α_1 is the rate of post-cracking stress decay as the strain increases, and α_2 is the sudden loss in stress at instant of cracking).

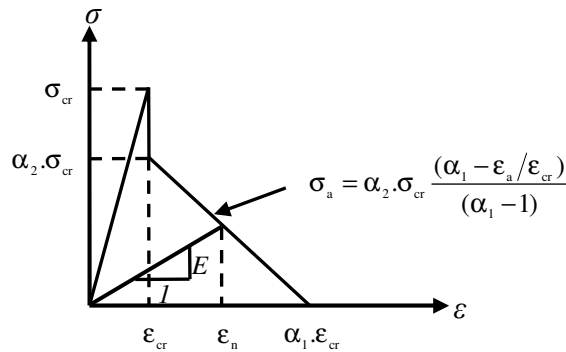


Fig. 5 Post-cracking for concrete in tension^[3].

In the finite element analysis of reinforced concrete members, a **shear retention model** is usually used. The shear stiffness at a cracked sampling point becomes progressively smaller as the crack widens. So the shear modulus of elasticity is reduced to βG . Before cracking the factor β is set equal to 1.0. When the cracks propagate, the shear reduction factor β is assumed to decrease linearly, Fig. 6^[21]. When the crack is sufficiently opened, a constant value is assigned to β , to account for the dowel action. The following relations are used to account for the shear retention effect.

$$1) \beta = 1.0 \text{ for } \epsilon_n \leq \epsilon_{cr}$$

$$(23)$$

$$2) \beta = \frac{(\gamma_2 - \gamma_3)}{(\gamma_1 - 1.0)} \left(\gamma_1 - \frac{\epsilon_n}{\epsilon_{cr}} \right) + \gamma_3 \text{ for } \epsilon_{cr} \leq \epsilon_n \leq \gamma_1 \epsilon_{cr} \quad (24)$$

$$3) \beta = \gamma_3 \text{ for } \epsilon_n > \gamma_1 \epsilon_{cr}$$

$$(25)$$

where, γ_1, γ_2 and γ_3 are the shear retention parameters., γ_1 , represents the rate of decay of shear stiffness as the crack widens, γ_2 , represents the sudden loss in the shear stiffness at the onset of cracking, and γ_3 , represents the residual shear stiffness due to the dowel action.

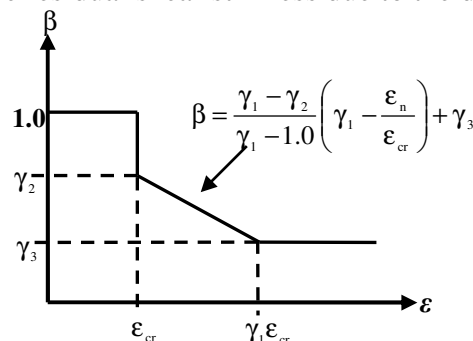


Fig. 6 Shear retention model for concrete^[3].

Modeling of Reinforcement

Modeling of reinforcing and prestressing steel in connection with the finite element analysis of reinforced and prestressed concrete members is much simpler than the modeling of concrete.

The reinforced and prestressed steel bars are long and relatively slender, and therefore, they can be assumed to transmit axial force only.

In the current work, an elastic-linear work hardening model is adopted to simulate the uniaxial stress-strain behavior of reinforcing and prestressing steel bars, Fig. 7.

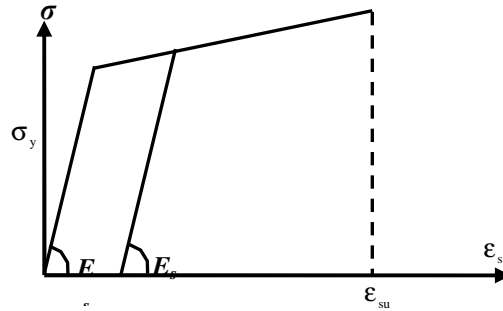


Fig. 7 Stress-strain relationship of reinforcing and prestressing steel bars.

FORMULATION OF PRESTRESSING

Equivalent Nodal Forces Method

Basic Assumptions

Few assumptions have to be made in order to obtain a workable mathematical model^[11].

1. The weakening of the concrete section by the holes provided for the prestressing tendons may be neglected.
2. The tension in the prestressing tendons is not affected by the elastic deformation of the structure.

Geometry of the Tendon and Variation of the Prestressing Forces

A particular brick element is considered where it is traversed by a prestressing tendon as shown in Fig. 8. The geometric definition of the tendon segment corresponding to a particular brick element is supposed to be of the following form^[11]:

$$X_c = \begin{Bmatrix} x_c \\ y_c \\ z_c \end{Bmatrix} = \sum_{i=1}^m M_i(\chi) \begin{Bmatrix} x_{ci} \\ y_{ci} \\ z_{ci} \end{Bmatrix} \quad (26)$$

In this equation, X_c stands for the vector of global Cartesian coordinates associated with a general point C situated on the axis of the tendon, χ is a non-dimensional parameter varying from -1 to +1 between the points of the segment, and x_{ci}, y_{ci}, z_{ci} ($i=1,2,\dots,m$) represent given Cartesian coordinates of m particular points C_1, C_2, \dots, C_m distributed as uniformly as possible on the axis of the tendon. The base function $M_i(\chi)$ associated with a particular node C_i , by taking a value of unity in C_i and zero at all other nodes $C_{k \neq i}$, is represented by Lagrange polynomial^[11]:

$$M_i(\chi) = \frac{(\chi - \chi_1) \dots (\chi - \chi_{i-1})(\chi - \chi_{i+1}) \dots (\chi - \chi_m)}{(\chi_i - \chi_1) \dots (\chi_i - \chi_{i-1})(\chi_i - \chi_{i+1}) \dots (\chi_i - \chi_m)} \quad (27)$$

The variation of tension $T = T(\chi)$ in the tendon is most adequately defined in the form consistent with the deflection of the tendon geometry, namely^[11]:

$$T = \sum_{i=1}^m M_i(\chi). T_i$$

(28)

where T_i ($i=1,2,\dots,m$) are given magnitudes of the tension at nodal points. They will be specified on the basis of the customary prediction of losses of the prestressing.

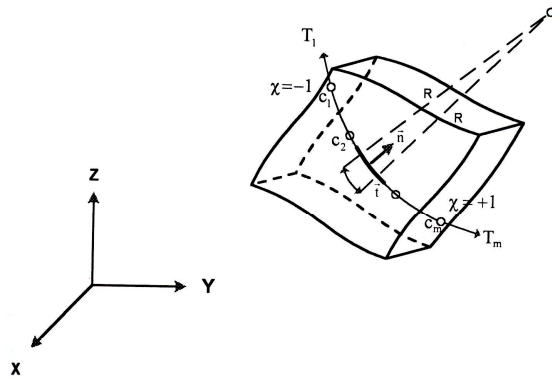


Fig.8 Typical segment of prestressing tendon traversing a brick element^[11].

Element Local Loads Due to Prestressing

The local action of a prestressing tendon on a particular brick element may be represented by a distributed line load acting on the element along the corresponding segment $C_1 C_m$ of the tendon axis and, if relevant, by a concentrated anchoring force applied to the element at the points (C_1, C_m) where the extremity of the tendon has been anchored in the concrete, as shown in Fig. 8.

The distributed line load has two components, the tangential component:

$$P_t = -\frac{dT}{ds} \tag{29}$$

and the normal component:

$$P_n = \frac{T}{R} \tag{30}$$

It is possible to combine the global components of the tangential and normal loads into a unique global Cartesian local vector:

$$p = \begin{Bmatrix} P_x \\ P_y \\ P_z \end{Bmatrix} = P_t t + P_n n \tag{31}$$

If one of the points C_1 or C_m of the tendon segment coincides with the end of the tendon, the end anchoring force $P_1 = T_1$ or $P_m = T_m$ (Fig. 8) must be applied to the element as a concentrated local load. This load, tangential to the tendon axis, will most conveniently be specified by giving the vector its Cartesian global components:

$$P_1 = \begin{Bmatrix} P_{x1} \\ P_{y1} \\ P_{z1} \end{Bmatrix} = (T.t)_{\chi=-1} \quad (32)$$

$$P_m = \begin{Bmatrix} P_{xm} \\ P_{ym} \\ P_{zm} \end{Bmatrix} = -(T.t)_{\chi=+1} \quad (33)$$

Vector of Primary Nodal Forces of the Element

The displacement definition of the brick element can be written as:

$$\{u\}_e = [N] \cdot \{a\}_e \quad (34)$$

and it is assumed that the element is traversed by only one prestressing tendon. Then, using the principle of virtual work, it can be shown that the local loads in Eqs. (31), (32) and (33) are balanced by the primary nodal forces of the element loads to^[17]:

$$\begin{aligned} [F_s] &= -\int_1 N^T(\xi_c, \eta_c, \zeta_c) P(\chi) ds - (N^T(\xi_{cl}, \eta_{cl}, \zeta_{cl}) P_1 \text{ or } \\ & N^T(\xi_{cm}, \eta_{cm}, \zeta_{cm}) P_m) \\ [F_s] &= -\int_1 N^T(\xi_c, \eta_c, \zeta_c) P(\chi) |V_t(\chi)| d\chi - \\ & (N^T(\xi_{cl}, \eta_{cl}, \zeta_{cl}) P_1 \text{ or } N^T(\xi_{cm}, \eta_{cm}, \zeta_{cm}) P_m) \end{aligned} \quad (35)$$

Lin's Method

Another method is used in the present study. This method is used to analyze the parabolic tendon in prestressed concrete box-girder bridges. The tendon is assumed to be frictionless and acts in the neutral plane of the brick element. The parabolic tendon may be replaced by two types of in-plane force: two end anchorage forces and a uniform pressure along the span of the bridge structure. Fig. 9 illustrates a curved post-tensioned tendon in a brick element.

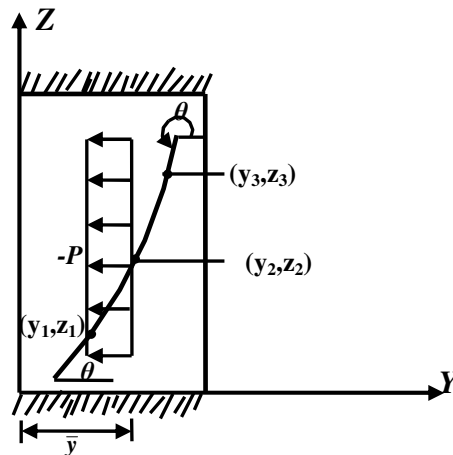


Fig. 9 Analysis of curved cable^[1].

This treatment of curved tendon follows the procedure used by Lin and applied by Loo and Cusens^[14].

The span of the cable is assumed to be parabolic and the total change of the slope is calculated as:

$$\vartheta = \tan^{-1}(B + 2C z_3) - \tan^{-1}(B + 2C z_1) \quad (36)$$

where:



$$C = \frac{\left(\frac{y_1 - y_2}{z_1 - z_2}\right) - \left(\frac{y_2 - y_3}{z_2 - z_3}\right)}{(z_1 - z_3)} \quad (37)$$

$$B = \frac{y_2 - y_3}{z_2 - z_3} - C(z_2 + z_3) \quad (38)$$

in which (y_1, z_1) , (y_2, z_2) and (y_3, z_3) are the coordinates for any three points in the parabolic curve spanning a brick element. The uniform pressure along the tendon duct may be replaced by a uniformly distributed in-plane load P along a line parallel to the z -axis, as shown in Fig. 9, and:

$$P = \frac{T\delta}{(z_3 - z_1)} \quad (39)$$

where T is the prestressing force in the tendon. The load is assumed to act as line \bar{y} , where:

$$\bar{y} = (y_1 + y_2 + y_3)/3 \quad (40)$$

In the present study, the uniform pressure is distributed equally upon the nodes for the elements spanning with parabolic tendon.

Short Term Prestress Losses

Frictional Losses

For post-tensioned members, the tendons are usually anchored at one end and stretched by jacks at the other end. As the steel slides through the duct, frictional resistance is developed, with the result that the tension at the anchored end is less than the tension at the jack. The total friction loss is the sum of the wobble friction due to unintentional misalignment, and the curvature friction due to the intentional curvature of the tendon. The following well-known equation is used to calculate the prestress loss at any point in the tendon at distance x from the anchorage end^[13]:

$$P = P_0 \cdot e^{-(\mu\alpha + \omega x)} \quad (41)$$

where, p_0 : force in jack end ($x=0$).

p : force in tendon at distance x .

μ : curvature friction coefficient.

α : angle change in prestressing tendon over distance x .

ω : wobble friction coefficient.

For parabolic profiles of constant curvature, Eq. (41) can be written as follows:

$$p = p_0 \cdot e^{-qx} \quad (42)$$

where $q = \mu\alpha + \omega$, q constant profile curvature ($\alpha = ax$).

Anchoring Losses

Prestress loss due to slip-in of the tendon when the prestress jack end is released is present in post-tensioned as well as pretensioned construction. Although it has a negligible effect on long tendons, it may become very significant for short tendons. However, anchor slip loss is mostly confined to a region close to the jacking anchorage. Distribution along the tendon is prevented by reverse friction as the tendon slips inward, and the steel stress throughout much of the tendon length may be unaffected by anchorage slip, Fig. 10.

Haug^[10] proposed a method for solving this problem. The force p_2 and length l_a over which anchor slip takes place are unknown. Considering the fact that the area under the curve

represents the elongation of the tendon, the following equation containing the unknown length l_a can be obtained:

$$l_a = \frac{2\Delta_s A_s E_s}{p_o(1 - e^{-2ql_a})} \quad (43)$$

where, Δ_s , is prestressing tendon anchor slip, A_s , is prestressing tendon area, E_s , is prestressing tendon modulus of elasticity.

Using Eq. (43), length l_a can be evaluated by using ordinary nonlinear solvers such as the iterative Newton-Raphson algorithm.

As shown in Fig. 10 the force in the tendon is then calculated as follows:

$$p = p_o \cdot e^{-q(2l_a - x)} \quad x \leq l_a \quad (44)$$

$$p = p_o \cdot e^{-qx} \quad x > l_a \quad (45)$$

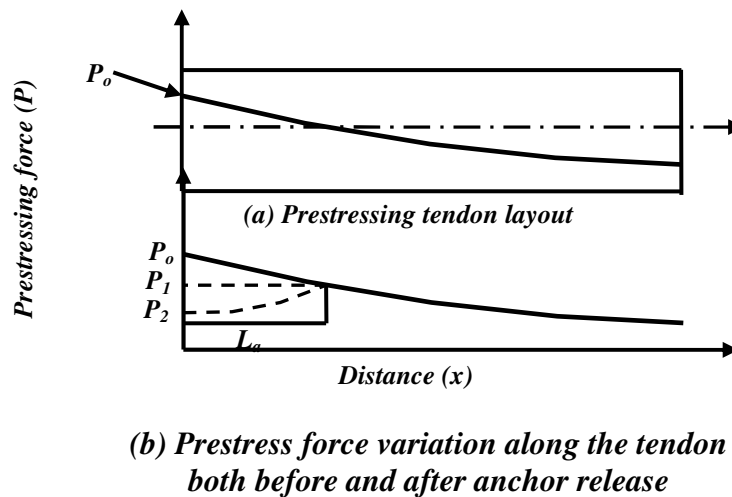


Fig.10 Prestress forces losses due to anchor slip^[9].

Computer Program

In the present study, the computer program P3DNFEA (Three-Dimensional Non-linear Finite Element Analysis), has been adopted. The program was originally developed by A-Shaarbaf^[3]. The main objective of the program is to analysis prestressed concrete box-girder bridges. Modifications and newly added subroutines were necessary to incorporate the effect of prestressing forces. The program is coded in FORTRAN 77 language.

APPLICATIONS AND RESULTS

The present nonlinear finite element model is used to investigate the behavior and ultimate load capacity of prestressed concrete box girders subjected to nonproportional loads and initial prestressing forces. Several examples are considered.

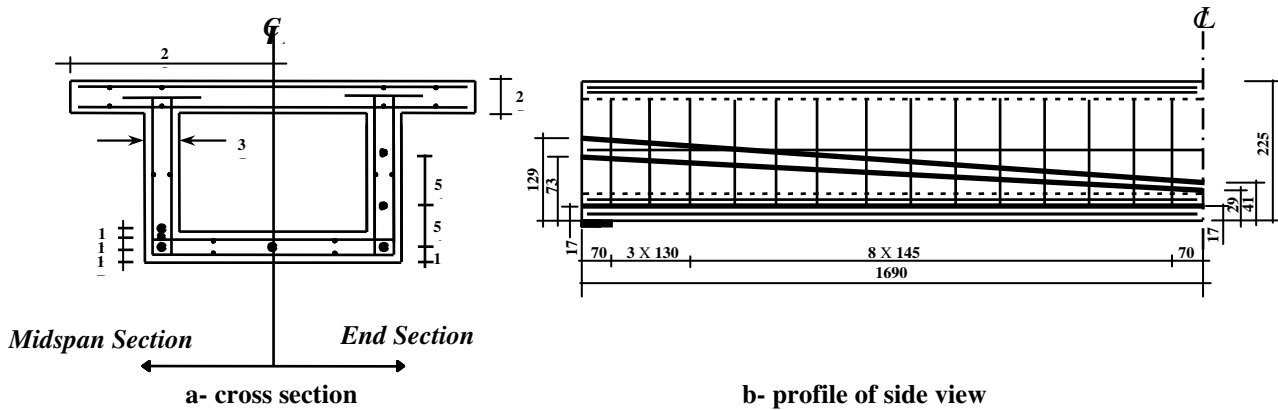
Simply Supported Single-Cell Prestressed Concrete Box-Girder Bridge

One-seventh scale model of a single-cell prestressed box-girder bridge^[19], simply supported at its ends is analyzed by using the present nonlinear finite element technique.

The geometry and finite element mesh are shown in Figs. 11 and 12. The applied loading for the bridge was considered to be of a scaled modeled of the Ontario Highway Bridge Design truck

(OHBDC) as shown in Fig. 13. The positioning of the trucks on the bridge model is shown in Fig. 12. The material properties of the concrete, reinforcing and prestressing steel are listed in Table 1.

Since the one-cell box-girder was symmetrically loaded with respect to its longitudinal axis, only one-half of the box-girder is modeled. The one-half structure has been modeled by 252 brick elements with a total number of 1815 nodal points, as shown in Fig. 12.



All dimensions in mm

Fig. 11 Structural details of the one-cell box-girder bridge

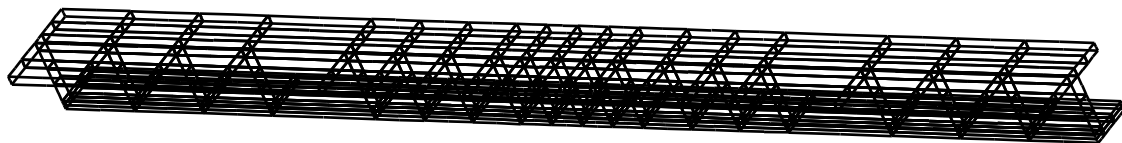


Fig. 12 Finite element idealization for half bridge model of one-cell box-girder

Table 1 Material properties of the one-cell box-girder bridge.

Concrete		Steel		
			prestressing	reinforcing
Elastic modulus, E_c (MPa)	22552	Elastic modulus, E_s (MPa)	180000	200000
Compressive strength, f_c' (MPa)	30	Yield stress, f_y (MPa)	1050.0	480.0
Tensile strength, f_t (MPa)	1.75*	Diameter (mm)	5.00	1.59
Poisson's ratio, ν	0.15*	Bar area, (mm ²)	19.6	2.00
Compressive strain at f_c'	0.0018	Ultimate strain	0.035	0.018
Ultimate compressive strain	0.0045	Yield strain	0.0035	0.0018
Cracking tensile strain	0.0002*	Poisson's ratio	0.3*	0.3*
		Initial prestressing force, P_o (kN)	14.406*	

*assumed
 $P_o = 0.7 A_p f_y$

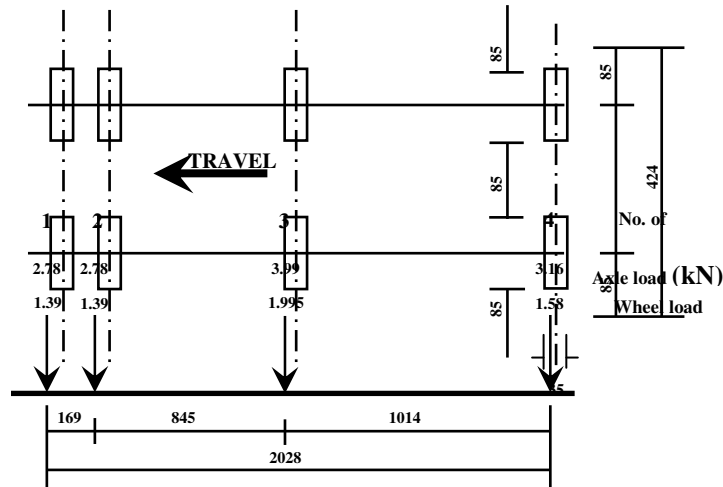


Fig. 13 Simulated Ontario Highway Bridge Design trucks (OHBDC) for one-cell box-girder bridge

Fig. 14 gives the load-midspan deflection curve of the prestressed box-girder bridge. The obtained results show close agreement in comparison with the experimental results. Fig. 15 shows the deflected shape of the bridge at various load levels. The level of the load is indicated by the ratio P/P_u , where P is the load at which the deflection is evaluated and P_u is the ultimate load for the bridge. The concrete longitudinal normal stresses at various locations in the bridge are illustrated in Figs. 16, 17 and 18. Fig. 16 and Fig. 17 show the longitudinal normal stress in the centerline of the top slab at midspan and quarterspan versus the level of load. Generally, the obtained results were nearly close to the experimental results. The variation of concrete longitudinal normal stresses along the centerline of the top slab is shown in Fig. 18. Figs 19 and 20 show the variation of longitudinal normal stress at cross-sections at midspan and quarterspan for the bridge at load ratio P/P_u equal to 0.250 and 0.8.

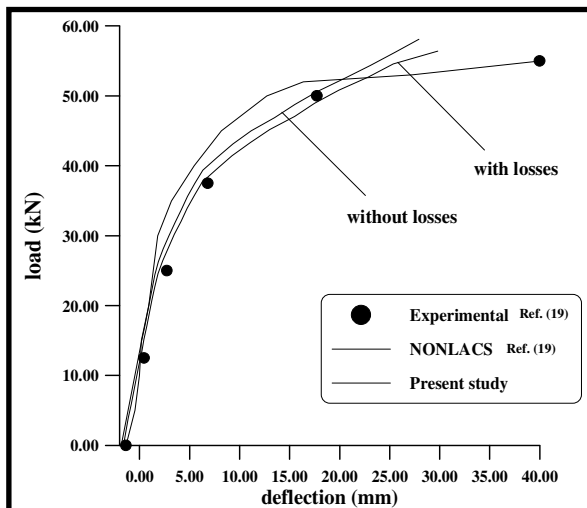


Fig. 14 Analytical and experimental load-midspan deflection curve for one-cell box-girder bridge

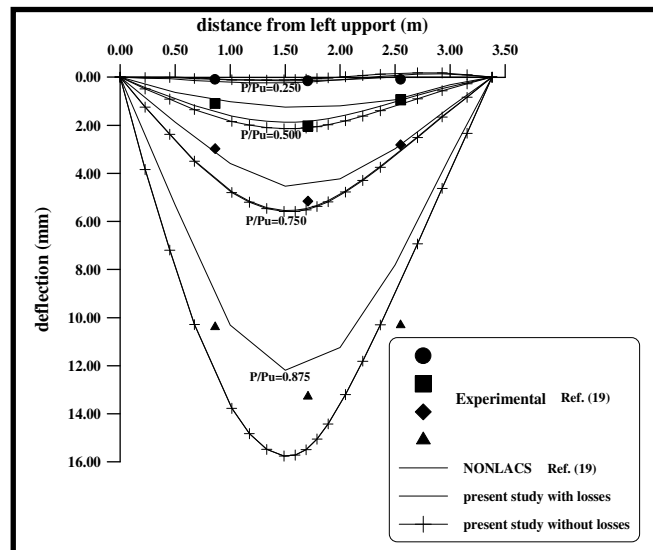


Fig. 15 Deflected shape of the bridge at various load levels for one-cell box-girder bridge

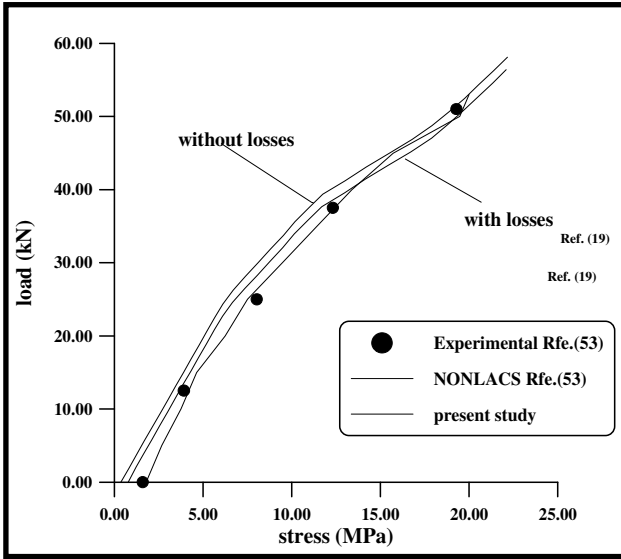


Fig. 16 Longitudinal normal stress on the top slab at midspan for one-cell box-girder bridge

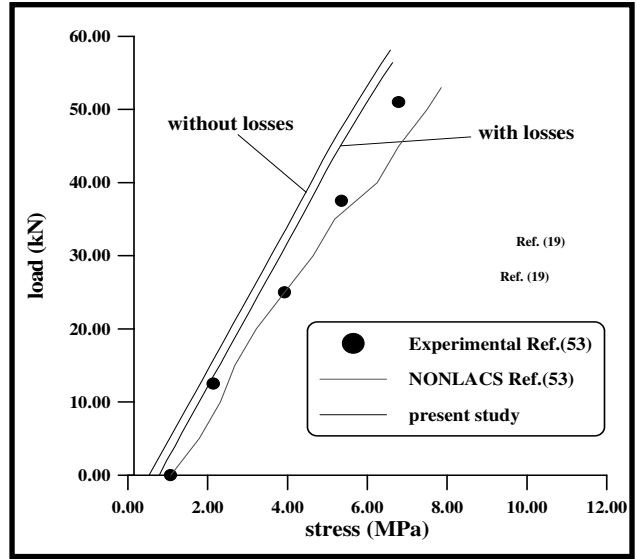


Fig. 17 Longitudinal normal stress on the top slab at quarterspan for one-cell box-girder bridge

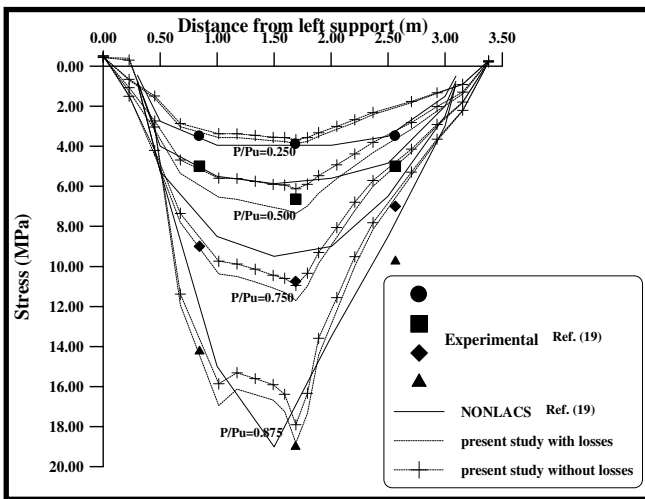


Fig. 18 Variation of concrete longitudinal normal stress along the centerline of the top slab for one-cell box-girder bridge

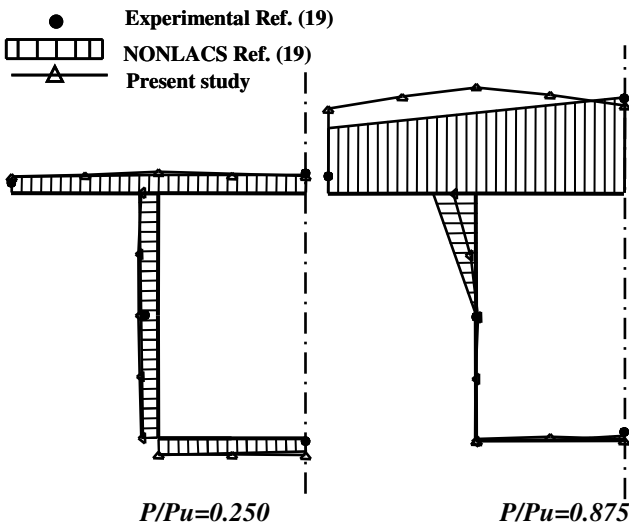


Fig. 19 Longitudinal normal stress variation across the section at midspan for one-cell box-girder bridge

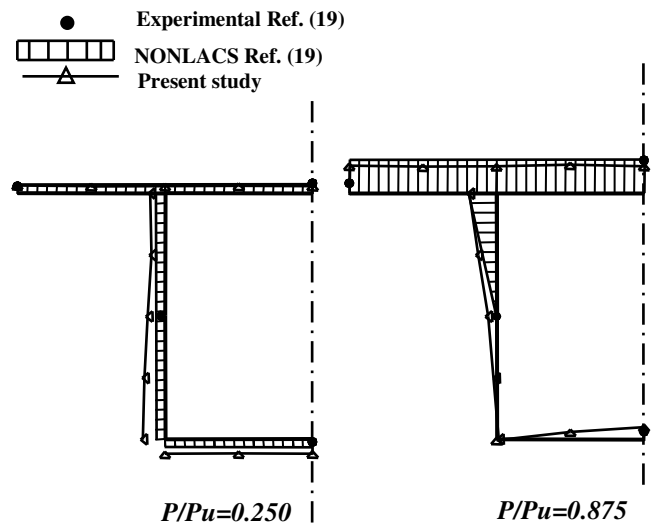


Fig. 20 Longitudinal normal stress variation across the section of slab at quarter span for one-cell box-girder bridge

Simply Supported Two-Cell Prestressed Concrete Box-Girder Bridge

The same authors^[53] of the previous example tested and analyzed another example. It was a two-cell box-girder, simply supported at its two ends.

The geometry and the finite element mesh are shown in Figs. 21 and 22. The applied loading for the bridge is shown in Fig. 23. The positioning of the trucks on the bridge model is shown in Fig. 22. The material properties of concrete, and reinforcing and prestressing steel are listed in Table 2.

One- half of the bridge is modeled due to the symmetry of loading with respect to the longitudinal axis. The two-cell box-girder was modeled with 308 brick elements with a total number of 2266 nodal points, as shown in Fig. 22.

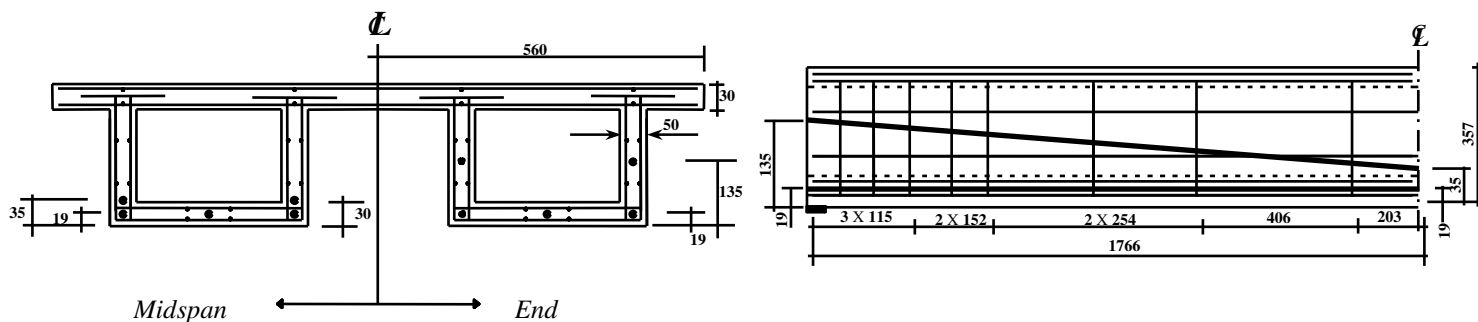


Fig. 21 Structural details of the two-cell box-girder bridge

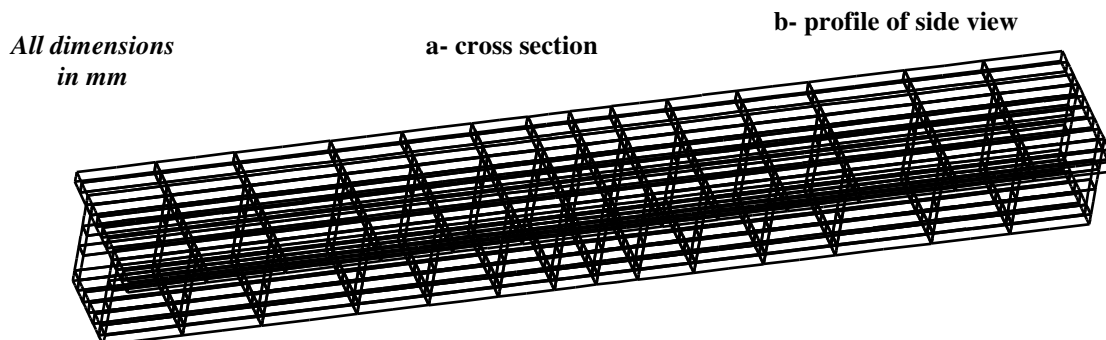


Fig. 22 Finite element idealization of half bridge model of two-cell box-girder

Table 2 Material properties of the two-cell box-girder bridge.

Concrete		Steel		
			prestressing	reinforcing
Elastic modulus, E_c (MPa)	28663	Elastic modulus, E_s (MPa)	175000	200000
Compressive strength, f_c' (MPa)	37	Yield stress, f_y (MPa)	1550.0	298.0
Tensile strength, f_t (MPa)	2.25*	Diameter (mm)	5.00	4
Poisson's ratio, ν	0.18*	Bar area, (mm ²)	19.6	12.90
Compressive strain at f_c'	0.0018	Ultimate strain	0.035	0.018
Ultimate compressive strain	0.0045	Yield strain	0.0035	0.0018
Cracking tensile strain	0.0002*	Poisson's ratio	0.3*	0.3*
		Initial prestressing force, P_o (kN)	21.266*	

*assumed

$$P_o = 0.7 A_{ps} f_y$$

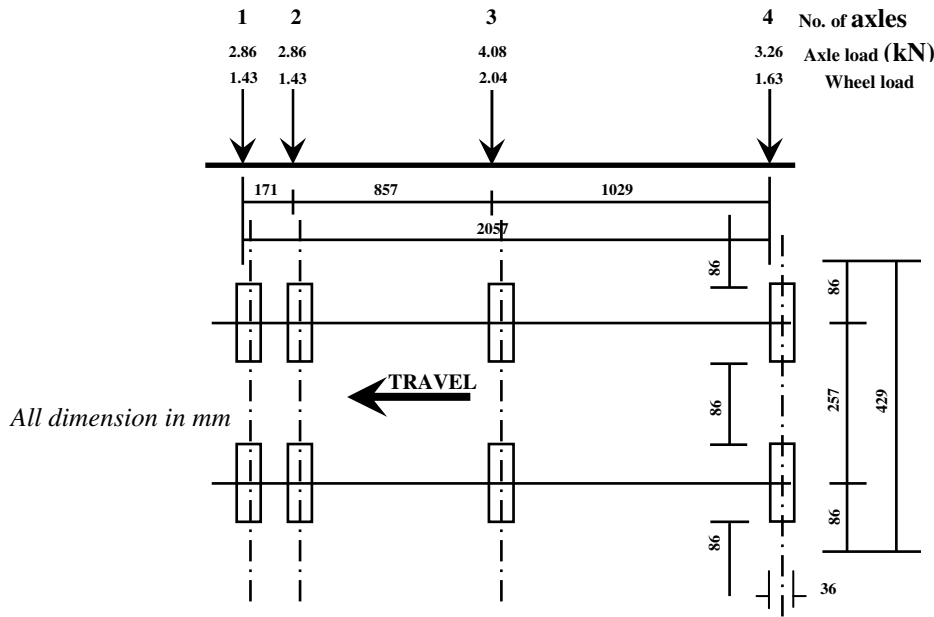


Fig. 23 Simulated Ontario Highway Bridge Design trucks (OHBD) for two-cell box-girder bridge

In Fig. 24, the load-deflection curve of the bridge is shown. Good agreement with experimental and NONLACS results is satisfied throughout most loading levels. The deflected shape due to external loading is shown in Fig. 25, it is measured at various levels of loading. The deflected shapes were measured along the longitudinal centerline of the bridge. Good agreement exists with the experimental results at various ratios of P/P_u , except the curve at the ratio $P/P_u=0.909$. Fig. 26 represents the development of longitudinal normal stress on the top slab at midspan versus the loading. It can be noted that the rate of development of stress is almost linear. The linear curve was due to the behavior of the structure. Generally, the obtained results are in good agreement with respect to the experimental and NONLACS results. A good agreement with respect to the experimental results at the top slab at quarter span of the bridge is also shown in Fig. 27. It can be noted that, the obtained results in the present study are more close to the experimental results than the NONLACS results. The variation of concrete longitudinal normal stresses along the centerline of the top slab is shown in Fig. 28. The comparison is fairly close with respect to the experimental results. Figs. 29 and 30 show the variation of longitudinal normal stress at the cross-section at midspan and quarter span for the bridge at a ratio P/P_u equal to 0.182 and 0.727.

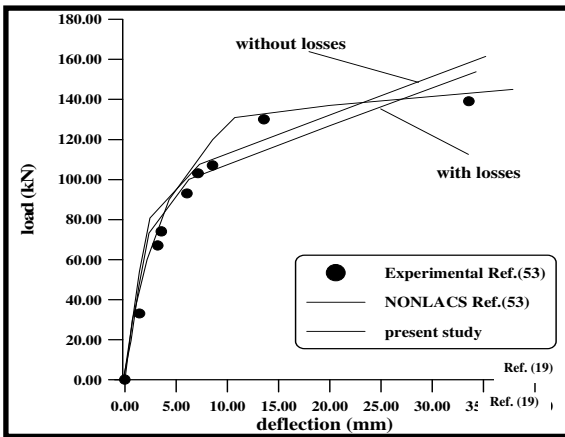


Fig. 24 Analytical and experimental load-midspan deflection curves for two-cell box-girder bridge

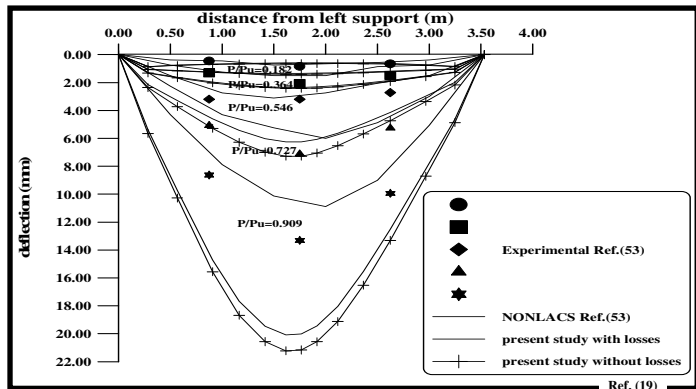


Fig. 25 Deflected shape of the bridge at various load levels for two-cell girder bridge

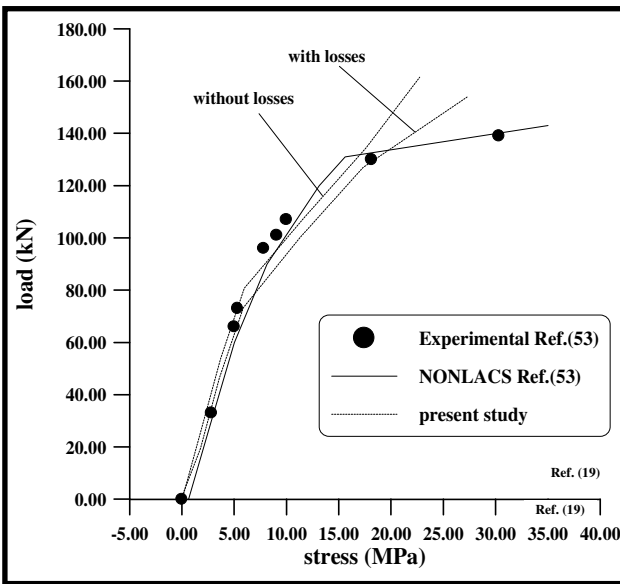


Fig. 27 Longitudinal normal stress on the top slab at quarter span for two-cell box-girder bridge

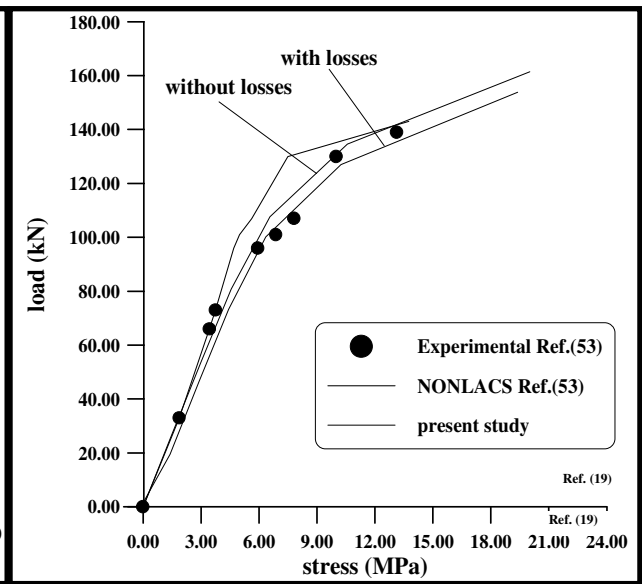


Fig. 26 Longitudinal normal stress on the top slab at midspan for two-cell box-girder bridge

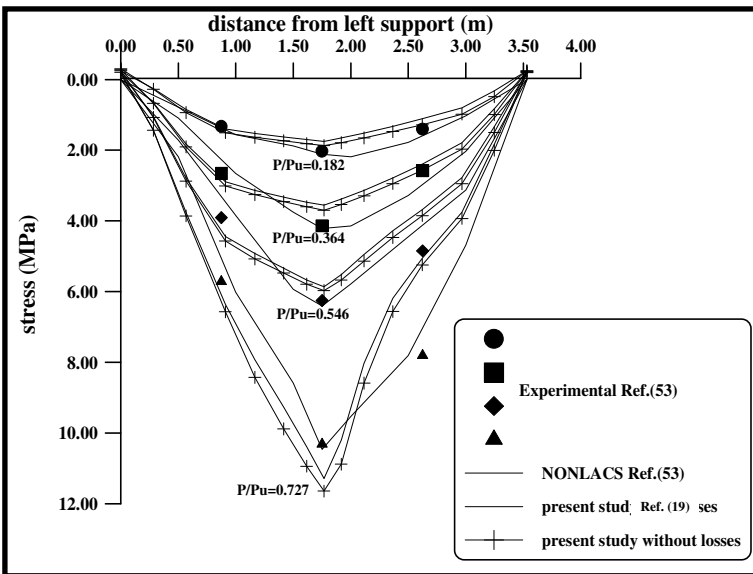


Fig. 28 Variation of concrete longitudinal normal stresses along the top slab for two-cell box-girder bridge

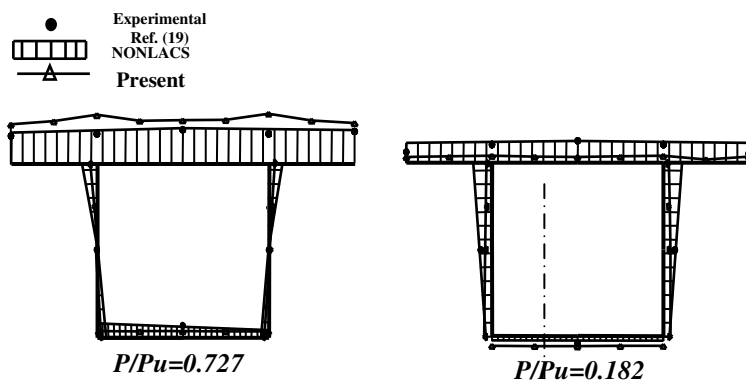


Fig. 29 Longitudinal normal stress variation across the section at midspan for two-cell box-girder bridge

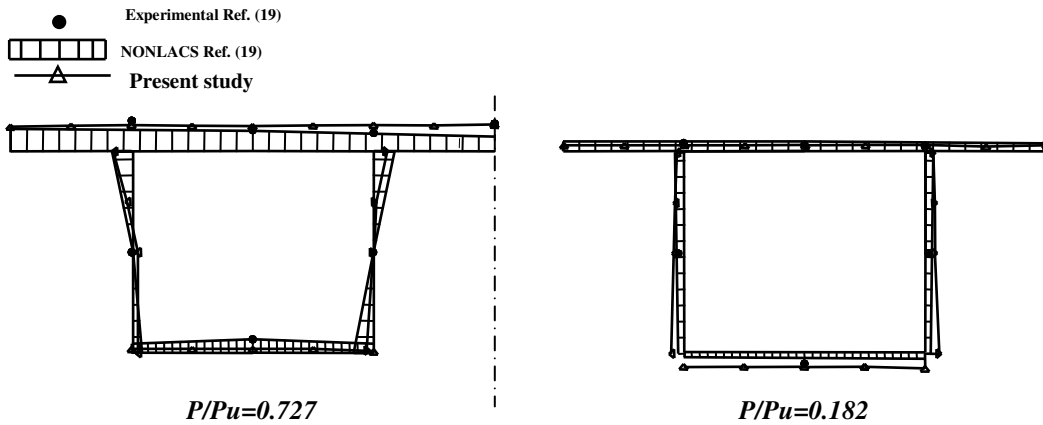


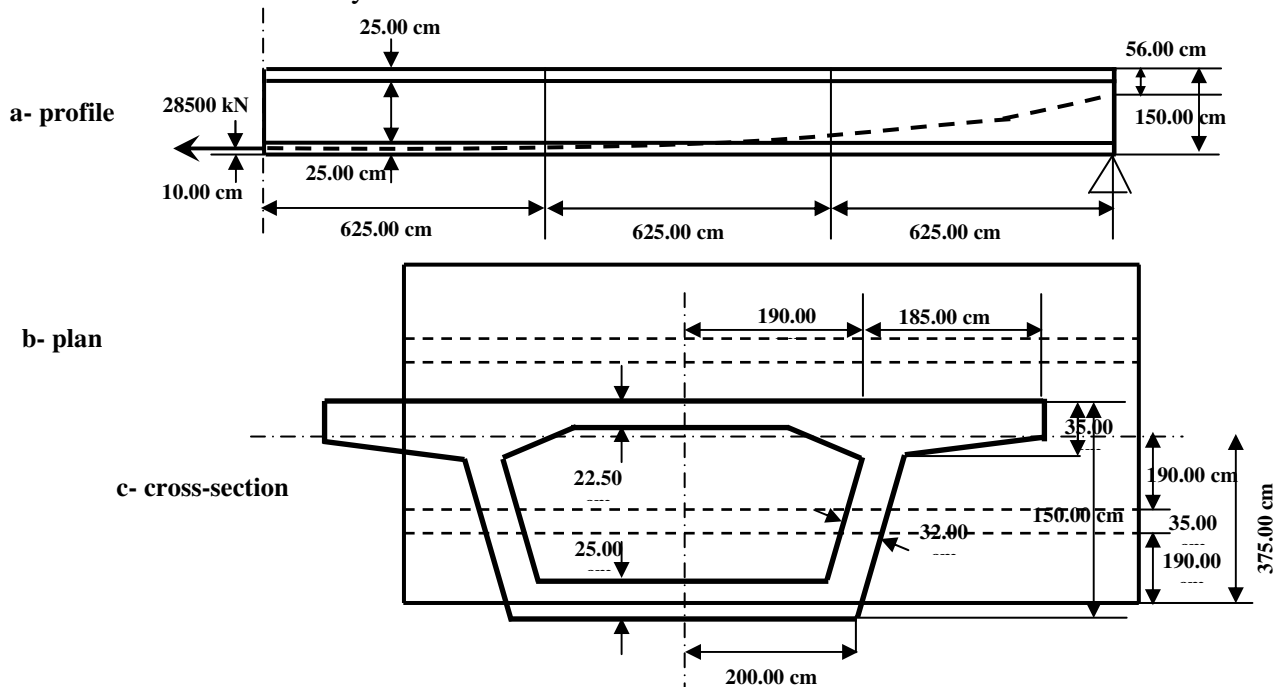
Fig. 30 Longitudinal normal stress variation across the section at quarter span for two-cell box-girder bridge

5.3 Simply Supported Single-Cell Prestressed Concrete Box-Girder with Inclined Web

A longitudinally prestressed single-cell box-girder, simply supported at both ends was analyzed by Jirousek et al^[11]. The box-girder is longitudinally prestressed by parabolic tendons located within the inclined webs. The profile of the tendons and geometry of the bridge model are shown in Fig. 31. The material properties of the bridge model are listed in Table 3. Each web of the bridge is provided with one-parabolic cable as shown in Fig. 31. The intensity of cable tension was assumed constant.

Due to symmetry of loading and geometry, one half of the bridge span was modeled with 176 brick elements and 1312 nodal points as shown in Fig. 32. In this example, the procedure used by Lin^[13] and applied by Loo and Cusens^[14] is used to represent the prestressing forces at the nodes.

Fig. 33 shows the vertical deflections for the cross-section at midspan due to prestressing forces only. Good agreement is obtained by comparing with Jirousek et al^[11] and Al-Temimi^[4] solutions. In Fig. 34, the distribution of longitudinal stresses at cross-section at midspan is shown. The obtained results are fairly close to Jirousek et al^[11] solution.



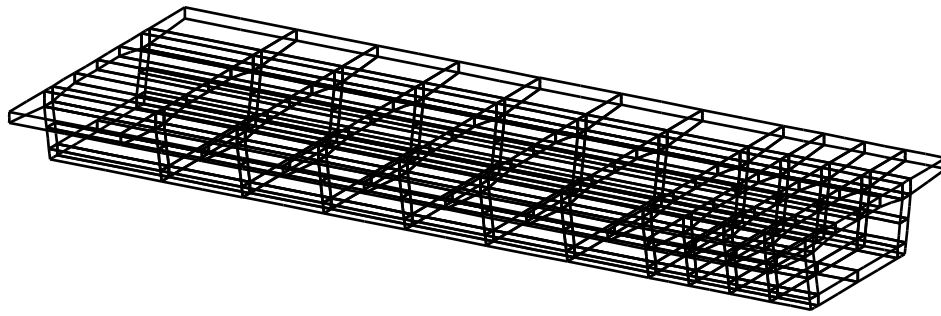


Fig. 32 Finite element mesh for the bridge model (half span)

Table 3 Material properties for the prestressed box-girder bridge with inclined webs.

Concrete							
Elastic modulus, E_c (MPa)	Compressive strength, f_c' (MPa)	Tensile strength, f_t (MPa)	Poisson's ratio, ν	Compressive strain at f_c'	Ultimate compressive strain	Cracking tensile strain	Initial prestressing force, P_o (kN)
29000	33.64*	3.132*	0.15	0.0018*	0.0045*	0.0002*	28500

*assumed

$$E_c = 5000 \sqrt{f_c'}$$

$$f_t = 0.54 \sqrt{f_c'}$$

- Jirousek Ref.(11)
- Al-Temimi Ref. (4)
- △— Present study

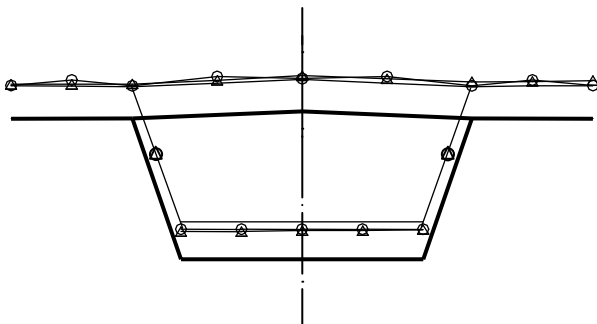


Fig. 33 Deflection of midspan cross-section

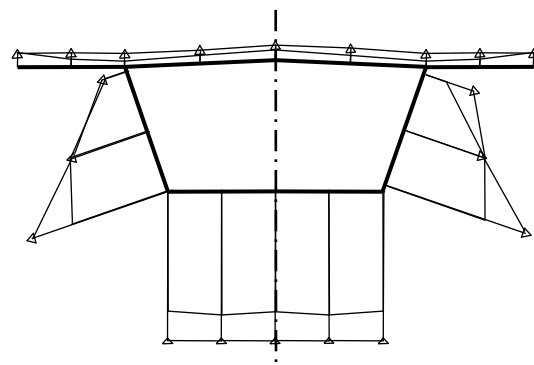


Fig. 34 Longitudinal stresses at cross-section midspan

CONCLUSIONS

The nonlinear finite element method is used to analyze prestressed concrete box-girder bridges. Based on the numerical analyses carried out, the following conclusions can be drawn.

1. The three-dimensional finite element model used in the present work is suitable to predict the behavior of prestressed concrete box-girder bridges under flexure. The numerical results



- showed the predicted load-deflection behavior, load-stress behavior and collapse load in good agreement with experimental results.
2. The losses in prestressing forces used in the present work improved the obtained results when comparing with the experimental results.
 3. The concept of equivalent nodal forces used in the present study is capable to simulate the loads exerted by the prestressing tendon upon the structure with fair accuracy. Also, Lin's method is proved to be more suitable to simulate the forces by the parabolic tendons.
 4. The contribution of the prestressing tendon stiffness to the element stiffness is considered and found to have some effect.

REFERENCES

- 1) Abdulla M.A. and Abdul-Razzaq A.A., "*Finite Strip Analysis Of Prestressed Box-Girder*", Computers and Structures, Vol. 36, No. 5, pp.817-822, 1990.
- 2) Al-Sabah A.S.I., "*Non-Linear Time-Dependent Finite Element Analysis of Plane Reinforced Concrete Members*", M.Sc. Thesis, University of Baghdad, February 1983.
- 3) Al-Shaarbaf I., "*A Nonlinear Three-Dimensional Finite Element Analysis Program for Steel and Reinforced Concrete Beam in Torsion*", Ph.D. Thesis, University of Bradford, 1990.
- 4) Al-Temimi J.E.M., "*Analysis of Reinforced and Prestressed Concrete Box-Girder Bridges by Ahmad Degenerated Shell Element*", M.Sc. Thesis, University of Al-Mustansiria, 2002.
- 5) Al-Zahawi S.K., "*Nonlinear Finite Element Analysis of Reinforced Concrete Voided Slab Strips*", M.Sc. Thesis, University of Technology, 1999.
- 6) Cervenka V., "*Constitutive Model for Cracked Reinforced Concrete*", ACI Journal, Vol.82, No.6, pp.877-882, November-December 1985.
- 7) Chen W.F., "*Plasticity in Reinforced Concrete*", McGraw-Hill, 1982.
- 8) Dawe D. J., "*Matrix and Finite Element Displacement Analysis of Structures*", Clarendon Press, Oxford, 1984.
- 9) Ghalib A.M.A., "*Inelastic Finite Element Analysis of Prestressed Concrete Multi-Planar Systems*", M.Sc. Thesis, Department of Civil Engineering, University of Baghdad, 1990.
- 10) Haung T., "*Anchorage Take-Up Loss in Post-Tensioned Members*", PCI Journal, Vol.14, August 1969.
- 11) Jirousek J. and Bouberguig A., "*A Macro-Element Analysis of Prestressed Curved Box-Girder Bridges*", Computers and Structures, Vol.10, pp.467-482, 1979.
- 12) Kindeel Z.M.R., "*Nonlinear Finite Element Analysis of Reinforced Concrete Beam-Column Joints*", M.Sc. Thesis, University of Al-Mustansiria, July 2003.
- 13) Lin T.Y. and Burns N.A., "*Design of Prestressed Concrete Structures*", Third Edition, John Wiley and Sons, 1982.
- 14) Loo Y.C. and Cusens A.R., "*A Finite Strip Program for the Analysis of Box-Girder Bridges*", User Manual, CIRIA Report 127/7, Civil Engineering Department, University of Dundee, 1972. (cited in Ref. 1)
- 15) Nilson A.H. and Darwin D., "*Design of Concrete Structure*", Twelfth Edition, 1997.
- 16) Nilson A.H., "*Internal Measurement of Bond Slip*", ACI Journal, No.69, pp.439-441, July 1972.
- 17) Owen D. R. and Hinton E., "*Finite Element in Plasticity, Theory and Practice*", Pineridge Press, Swansea, U. K. 1980.
- 18) Pagnani T., Slater J., Aneur-Mosor R. and Boyukourk O., "*A Nonlinear Three-Dimensional Analysis of Reinforced Concrete Beam on Boundary Surface Model*", Computers and Structures, Vol.43, No.1, pp.1-12, 1992.

- 19) Razaqpur A.G., Nofal M. and Mirza M.S., “*Nonlinear Analysis Of Prestressed Concrete Box-Girder Bridges Under Flexure*”, Canadian Journal of Civil Engineering, Vol. 16, pp.845-853, 1989.
- 20) Schlaich J. and Seheel H., “*Concrete Box-Girder Bridges*”, International Association for Bridge and Structural Engineers, Swiss, 1982.
- 21) Zeinkiewicz O.C., “*The Finite Element Method*”, Third Edition, Mc Graw, Hill, London, 1977.